



Nitric oxide laser-induced fluorescence using the fifth harmonic of a broad-band Nd:YAG laser

Tom Bolderman¹ · Noud Maes¹ · Nico Dam¹

Received: 7 June 2024 / Accepted: 25 July 2024 / Published online: 1 August 2024
© The Author(s) 2024

Abstract

We explore the prospects of laser-induced fluorescence diagnostics of nitric oxide (NO) using non-tunable fifth-harmonic radiation of a broad-band, ns-pulsed Nd:YAG laser at $\lambda = 213$ nm. Typically, 2–5 mJ/pulse of 213-nm radiation is produced by a commercial harmonic generator in this study, with an efficiency of about 1–3% (relative to the input pulse energy). We present spectral results obtained in various environments, ranging from air-based combustion processes at room conditions up to elevated pressure and temperature environments, the latter resembling conditions typical for compression-ignition internal combustion engines. In all cases, the laser-induced fluorescence spectrum shows clear signatures of the NO spectrum, mostly on transitions in the γ -band system ($A^2\Sigma^+ \rightarrow X^2\Pi$). At higher fluences, multi-photon absorption also gives rise to blue-shifted fluorescence. The fluorescence yield increases with increasing pressure, allegedly due to non-resonant excitation, the efficiency of which increases with increasing pressure broadening. When applied to air-based combustion processes, interference by (hot) oxygen needs to be taken into account. We conclude that the method is a relatively straightforward option to visualize the NO distribution in a broad variety of applications.

1 Introduction

The potential formation of nitric oxide (NO) is a point of concern in all combustion processes involving air as oxidizer (or high-temperature air in general). Thus, the experimental visualization of NO distributions in combustion devices has received considerable attention [1–3]. Because of its non-intrusive nature, Laser-Induced Fluorescence (LIF) has become the experimental visualization technique of choice, typically employing some kind of tunable, pulsed laser system for excitation and intensified CCD cameras for detection.

Compression-ignition internal combustion engines, infamous for their soot-NO_x trade-off, belong to the most ubiquitous combustion systems in (past and) current use.

(See [4] for an early review of nitric oxide formation in these devices.) A number of studies have successfully applied NO LIF in engine-like environments using various excitation strategies, mainly in the $A^2\Sigma^+ - X^2\Pi$ band system (also known as the γ -bands) or in the $D^2\Sigma^+ - X^2\Pi$ band system. In the latter case, a tunable ArF excimer laser is tuned to one of the transitions in the 193-nm range, but this deep UV radiation suffers from severe attenuation due to absorption by O₂ and CO₂ in the high-pressure, high-temperature conditions typical for internal combustion engines [5, 6]. Attenuation is less of an issue when excitation takes place in the γ -bands (at 226 nm or larger wavelengths), employing a frequency-doubled dye laser or an optical parametric oscillator (OPO) for excitation. In a comparative study [2, 7, 8], Bessler et al. identified the $A \leftarrow X(0,0)$ excitation scheme as the most advantageous approach for NO visualization, in terms of signal strength and spectral purity, with only limited temperature dependence. At an excitation wavelength of 226 nm this approach still suffers from attenuation. An alternative approach, involving excitation in the $A \leftarrow X(0,2)$ band using a tunable KrF excimer laser [9], suffers less from attenuation, but the price to pay is sensitivity to hot NO only. In all these cases, the laser systems needed for fluorescence excitation are relatively complicated and expensive, requiring skilled operators for proper execution of the experiments.

✉ Nico Dam
n.j.dam@tue.nl
Tom Bolderman
tombolderman@hotmail.com
Noud Maes
n.c.j.maes@tue.nl

¹ Mechanical engineering, Eindhoven University of Technology, Box 513, 5600 MB Eindhoven, The Netherlands

Still, new developments in NO detection strategies regularly appear in literature [10–16], in part stimulated by new combustion concepts [17–19]. In this paper we explore an alternative approach to the visualization of NO, using the 5th harmonic radiation of an unseeded, ns-pulsed Nd:YAG laser for excitation. This type of Nd:YAG laser is ubiquitous in combustion and fluid dynamics laboratories worldwide, and 5th harmonic boxes are commercially available, cost-effective, and straightforward to operate. The fundamental wavelength of the Nd:YAG laser, at 1064.15 nm [20] (1064 nm for short), can thus be quintupled to obtain 212.83-nm radiation (213 nm for short). Based on simulations performed with LIFBASE [21], excitation in the $A \leftarrow X(1,0)$ and $(2,1)$ bands should be possible with this wavelength, also at atmospheric pressure and temperature conditions; see Fig. 1. At higher temperature and/or pressure, the excitation efficiency is expected to increase, due to better overlap of the excitation wavelength with available transitions, either because more lower states become populated, or because linewidths increase. In the context of standoff detection of nitrotoluenes, Arnold et al. [11] have already demonstrated the possibility of exciting NO in the γ -bands, either at ambient conditions or as photolysis product of nitrotoluene, by means of frequency-quintupled Nd:YAG laser radiation.

Here, we present measurements of NO under ambient conditions as well as in high-pressure and/or high-temperature environments, using the 5th harmonic of a broad-band Nd:YAG laser for excitation and a grating spectrograph for

detection. Spectral filters could be used for 2-D imaging, but here we focus on the spectral signature of NO. This study does not explore quantification of the NO_x distribution; this would require a calibration, like any other LIF implementation. Rather, we merely intend to point out that a relatively simple extension of the laboratory work-horse Nd:YAG laser opens up the possibility to study one of the most important potential pollutants of any air-based combustion process, nitric oxide.

2 Experimental methods

In this work, the 5th harmonic of the fundamental output of an unseeded, ns-pulsed Nd:YAG laser (Quanta Ray PRO-250, Spectra Physics) is created in an Ekspla H300FiHC harmonic generator. The generator contains two doubling crystals to subsequently generate 532-nm and 266-nm radiation, followed by a mixing crystal that combines the 266-nm radiation with the residual fundamental radiation at 1064 nm by sum frequency generation. This results in up to 30 mJ/pulse at 213 nm with a fundamental input of 800 mJ. Conversion efficiency decreases with decreasing input pulse energy. Based on manufacturer information, we expect the pulse duration of the 5th harmonic to be ca. 5 ns and its frequency bandwidth to be $< 4 \text{ cm}^{-1}$.

Fluorescence from the sample of interest is observed under 90°, through a 64-mm f/2 UV objective lens (Bernhard

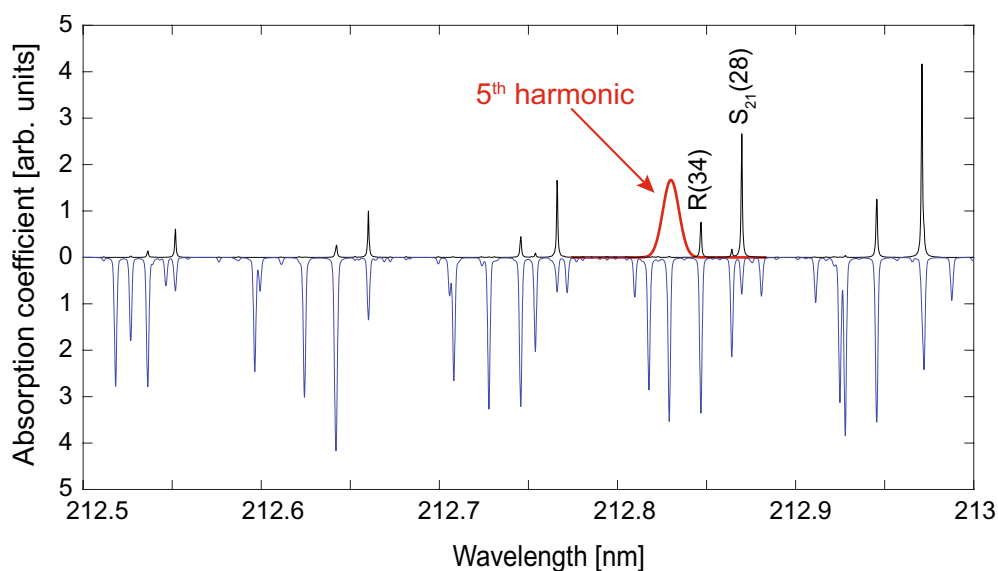


Fig. 1 LIFBASE simulations of the NO absorption spectrum in the $A \leftarrow X$ band system, in the wavelength range of the 5th harmonic of the Nd:YAG laser. Two spectra are plotted here, back-to-back: black (facing upward) for a temperature of 300 K, and blue (facing downward) for a temperature of 2000 K. The spectra are scaled individually. The room temperature spectrum is dominated by absorption

lines in the $A \leftarrow X(1,0)$ band, the ‘hot’ spectrum is dominated by absorption lines in the $A \leftarrow X(2,1)$ band. In the upward-facing spectrum, the 5th harmonic of the Nd:YAG laser is indicated by the red bell-shaped curve, and the rotational assignment of the transitions contributing most to the room-temperature absorption is included

Halle Nachf.) mounted on an imaging grating spectrograph (Acton SpectraPro-300i) equipped with a UV-blazed 1200-gr/mm reflection grating and an intensified CCD (ICCD) camera (Roper PIMAX 1, SB-slow intensifier) on its exit port. Such a spectrograph images the entrance slit onto the exit port, each wavelength component of the incident light producing an image at a different location on the exit port [22]. In our experiments, the entrance slit of the spectrograph is aligned along the laser beam propagation direction, so that the spectrograph output images show spectral resolution along one axis (perpendicular to the entrance slit orientation) and spatial resolution along the laser beam along the other axis (parallel to the entrance slit). The camera opens with a gate width of 100 ns, starting at the laser pulse. Unless indicated otherwise, spectra shown in this paper are corrected for background and spectral sensitivity of the detection system.

To demonstrate the broad range of application of this NO visualisation method, we present data on NO in a gas cell at ambient temperature (293 K) and varying pressure (1–20 bar), in the burnt gas of an atmospheric-pressure oxygen-acetylene welding torch, and under engine-like conditions in a pre-burn combustion vessel. Details on these setups are provided below.

3 Results and discussion

3.1 Atmospheric pressure NO LIF

Figure 2 shows the spectrally resolved fluorescence following excitation of 400 ppm NO in N₂ bath gas at 1 bar and

20°C by about 2 mJ/pulse of 213-nm radiation. The sample gas is contained in a small pyrex cell, with fused quartz windows for laser beam passage and fluorescence observation. The spectra displayed in Fig. 2 are collages, made up of individually recorded spectra covering a 33-nm wide range and neighbouring spectra overlapping by 6.5 nm. Each recording is based on 1000 on-chip accumulations, and the individual recordings are stitched together by post-processing in Matlab[®]. The sample cell itself produces strong stray light (elastic scattering of the excitation laser beam), and therefore the spectral region around 213 nm is skipped in the measurements. Two fluorescence spectra are shown back-to-back, one (pointing downwards, blue) with unfocussed excitation laser beam, the other (pointing upwards, black) with the laser beam focussed into the probe volume by a 300-mm plano-convex lens. Both spectra are dominated by emission in the γ -bands. The unfocused laser beam excites transitions in the A(1) \leftarrow X(0) band, and the emission out of A(1) makes up most of the fluorescence, with only about 3.5% following prior relaxation down to A(0). The focused laser beam apparently induces multi-photon transitions, populating higher energy states that give rise to fluorescence that is blue-shifted relative to the excitation wavelength, as well as emission out of the A(2) state. The more prominent peaks between 180 and 213 nm correspond to the first few members of the C(0) \rightarrow X(v') progression.

Spectra recorded in the cone region of an atmospheric oxy-acetylene welding torch flame are qualitatively very similar to the gas cell spectra; see Fig. 3. The spectrum is dominated by emission out of the directly excited A(1) state, with relatively broad rotational envelopes (as compared to the room temperature spectra of Fig. 2). The

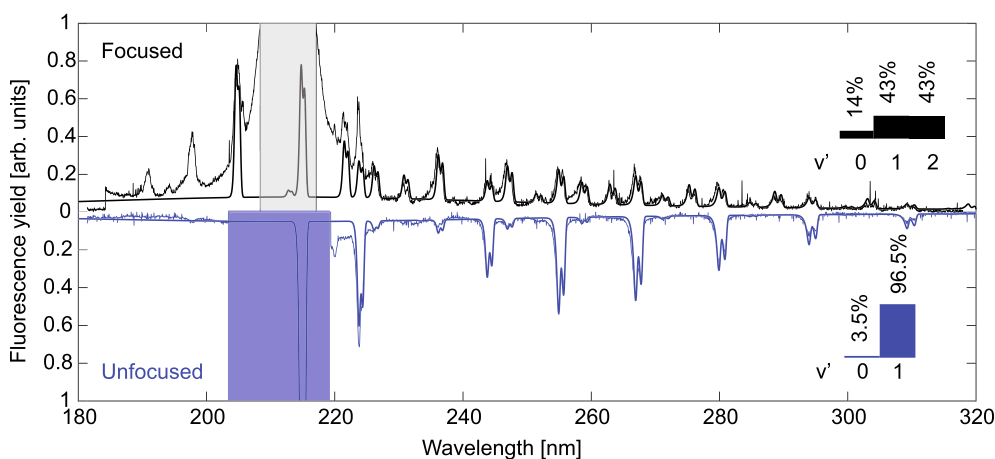


Fig. 2 Cell spectra (400 ppm NO in N₂, 1 bar, 293 K). Two fluorescence spectra are plotted back-to-back; the upward-pointing black spectrum is recorded following excitation by a focussed 213-nm beam, the downward-pointing blue spectrum is generated by an unfocussed excitation beam. The two spectra are scaled individually. In

both plots, the smooth curves with increased thickness show γ -band emission (A(v') \rightarrow X(v'')) based on LIFBASE simulations; the bar graphs at the right indicate the relative contributions of the various upper vibrational states

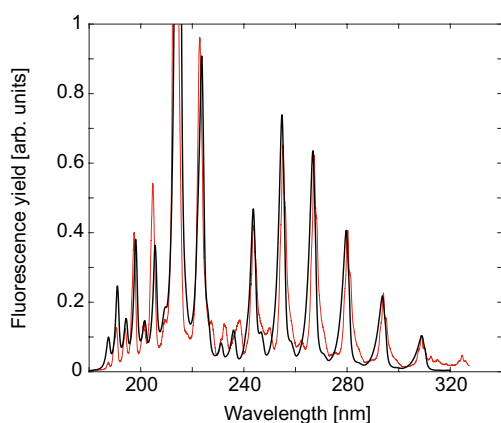


Fig. 3 Flame spectrum, recorded in the cone region of an oxy-acetylene welding torch, following excitation by a focussed 213-nm beam (thin red line). A simulation based on LIFBASE is included (the smooth, black curve); this is a compilation of LIFBASE-generated fluorescence spectra out of the D(0), C(0) and A(1) vibronic states, for a rotational temperature of 1500 K

almost complete absence of contributions from other vibrational states indicates that the higher temperature in the flame has populated rotational states in the electronic ground state(s) that are more efficiently excited by the 5th harmonic radiation at 213 nm, as compared to the room temperature case. The fluorescence that is blue-shifted relative to the excitation wavelength can be attributed to emission from the C(0) and D(0) states, which must have been reached by multi-photon absorption.

3.2 Pressure influence

The pressure dependence of the NO LIF spectrum is studied in an optically accessible pressure chamber, with small quartz windows on opposite sides to provide for laser beam access, and a large observation window in the perpendicular direction. For the latter, only a BK7-window was available, which limited the recorded fluorescence spectrum to wavelengths longer than about 300 nm. The vessel was initially filled with 2 bar of the same 400 ppm NO in N₂ mixture as was used for the spectra in Fig. 2, and subsequently pressurized, and diluted, by adding N₂. (That is, the NO number density stays the same, but its concentration decreases with pressure.) Spectra were recorded using a focussed excitation laser beam, as above, integrating 2000 laser pulses on the CCD sensor. Spectra at various pressures are shown in Fig. 4. The top panel shows the raw data recorded by the camera in a false color scale (20 bar total pressure); the spectra in the lower panel are extracted from similar 2-D spectra by column-wise summation of pixel rows between the two horizontal white lines; they are not corrected for the internal transmission of the observation window. The laser beam was focussed halfway between these white lines.

As in the case of the atmospheric cell spectra, the spectrum is dominated by emission out of the A(1) and A(0) states. The fluorescence yield is seen to increase with pressure, a somewhat unusual feature. Most likely, this is due to the excitation wavelength not being resonant with any transition. Absorption takes place in the wings of several individual transitions (see Fig. 1), and with increasing pressure broadening, the overlap between the absorption profile

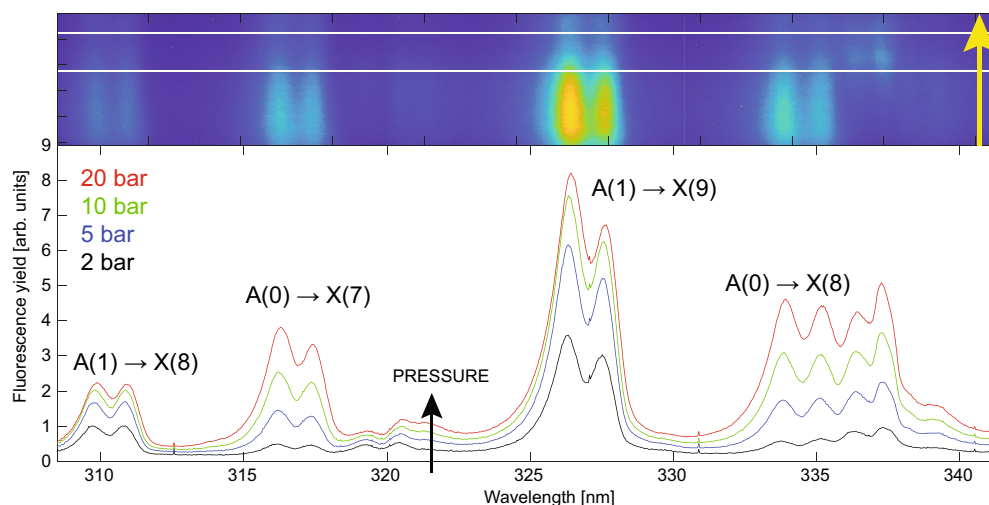


Fig. 4 Spectra recorded in a pressure vessel containing about 0.8 mbar NO in nitrogen (total pressure indicated at the left), following excitation by a focussed 213-nm beam. The upper panel shows a 2-D spectrum in false color; the wavelength axis is horizontal, the vertical axis is aligned with the laser beam (yellow arrow), which is

focussed halfway between the two horizontal white lines. The lower panel shows spectra derived from this and similar 2-D spectra, by summing the pixel rows between the two white lines. Note the emission around 337 nm, which is seen only at and around the focal point of the excitation laser

and the excitation laser profile improves. This is illustrated by Fig. 5, which shows the overlap integral η ,

$$\eta = \int_{-\infty}^{+\infty} \mathcal{L}(\lambda; \lambda_5) \mathcal{S}(\lambda) d\lambda, \quad (1)$$

of the 5th harmonic radiation (assumed to have a gaussian wavelength envelope \mathcal{L} centered at $\lambda_5 = 212.83$ nm) with the room-temperature NO absorption spectrum \mathcal{S} , for 5th harmonic bandwidths of 2 cm^{-1} (dashed curve) and 4 cm^{-1} (solid curve). When the pressure increases above atmospheric pressure, the increasing linewidth initially leads to better overlap with the laser bandwidth, up to a certain optimum. The steepness of this pressure dependence depends strongly on the details of the irradiation bandwidth and the absorption spectrum. Simultaneously, collisional relaxation rates increase with pressure, which reduces the fluorescence yield out of the directly excited A(1)-state, but less so for the fluorescence out of the A(0)-state, which is largely populated indirectly, by (collision-induced) vibrational relaxation out of the A(1)-state. In the focal point of the laser beam multi-photon processes start playing a role, giving rise to additional emission around 337 nm, possibly from the 2nd positive system of N_2 [24].

3.3 Engine-like environment

Finally, NO LIF with 213-nm excitation is tested in the optically accessible constant-volume combustion vessel, described in detail in [25, 26]. In this vessel,

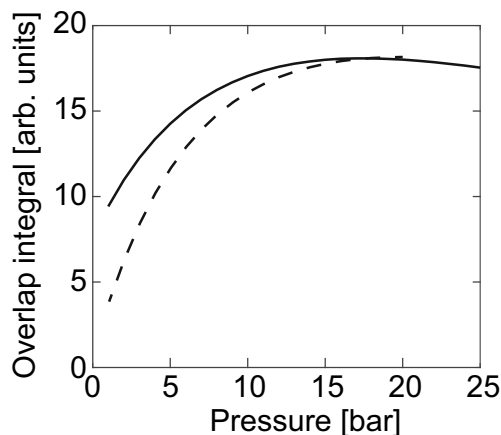


Fig. 5 Overlap integral of the 5th harmonic radiation of the broad-band Nd:YAG laser with the room-temperature NO absorption spectrum of Fig. 1 as a function of pressure. Data for pressure broadening and shift of the NO absorption lines have been taken from [23], assumed to be valid for absorption lines in the $A \leftarrow X(1, 0)$ band, too. The spectral profile of the 5th harmonic is taken to be gaussian, with a full width of 4 cm^{-1} (solid curve) and 2 cm^{-1} (dashed curve)

ambient conditions typical for heavy-duty internal combustion engines are achieved by igniting a combustible mixture (the so-called “pre-burn”). The composition of the pre-burn mixture is tailored such that the desired conditions (in terms of pressure, temperature, and oxygen concentration) are reached at some point during cool-down, at which moment a fuel spray can be injected into the pre-burn end gas. The optical diagnostics used for spray studies are focused at the center of the combustion vessel. Thus, the 213-nm beam has to travel about 50 mm through a high-pressure and high-temperature ambient before it reaches the fuel spray axis and the field of view of the detector. To compensate for the increased absorption losses, the laser pulse energy for these experiments was increased to about 5 mJ/pulse. Since our Nd:YAG laser has a 10-Hz pulse repetition rate, only one single measurement can be taken per fuel injection event. As compared to the (quasi-)stationary setups discussed above, this severely limits the practical possibilities for ensemble averaging.

Spectra recorded without spray flame at 22.8 kg/m^3 , 15% O_2 and temperature ranging between 800–1100 K were used to assess the background fluorescence by the ambient gas. At 1100 K the spectra are dominated by molecular oxygen fluorescence in the $B^3\Sigma_u^- \leftarrow X^3\Sigma_g^-$ Schumann-Runge bands, see Fig. 6. The intensities of both Rayleigh scattering and LIF significantly decrease along the laser beam propagation direction, indicating strong absorption (presumably by hot O_2 , NO, and possibly also hot CO_2 and H_2O [27]). At ambient temperatures of 900 K and lower, this absorption becomes much less significant, and most spectral structure originates from the fluorescence out of the NO A($v' = 1$) -state. Clearly, under the conditions in the pre-burn combustion vessel, both background fluorescence and laser beam attenuation should be taken into account.

Figure 7 shows the ensemble-averaged spectra of four or five experiments in the combustion vessel at so-called ‘Spray A’ boundary conditions [28], using n-dodecane ($\text{C}_{12}\text{H}_{26}$) as fuel. The typical structure of such spray flames can be found in the literature [26]. Spectra were recorded at 4.5 ms after start of injection (total injection duration 6 ms). The field of view covers about 20 mm on one side of – and including – the spray axis, 65 mm downstream of the nozzle exit; the laser beam passes top-down through the field of view. In Fig. 7 the top panels show the minimally processed data recorded by the spectrograph. The horizontal white-dashed lines indicate the radial extent of the spray flame at this location. (This was obtained from separate measurements, using a gate width of $2 \mu\text{s}$ and the spectrograph set to 400 nm center wavelength, to observe soot incandescence.) The bottom panel shows the spectrum obtained from integration over the full height of the upper panels. The short-wavelength part of the spectrum is saturated, due to strong Rayleigh scattering; the extent of the saturation decreases along

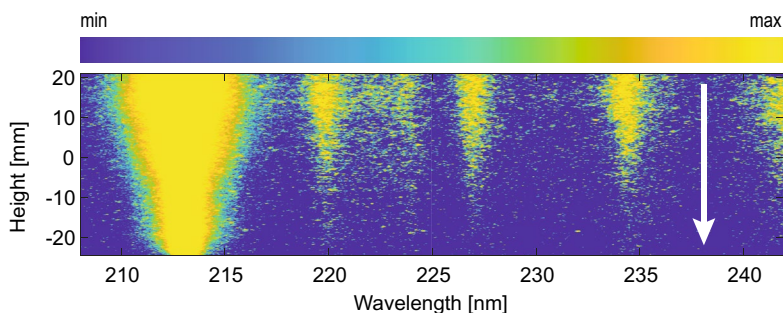


Fig. 6 Fluorescence spectrum recorded under 'Spray A' conditions in a pre-burn combustion vessel, recorded at 65 mm downstream of the nozzle exit (but without fuel spray). The laser beam passes the field of view top-down (white arrow). The spectrum is shown in a

false-color logarithmic scale, to emphasize the strong attenuation of the laser beam by the vessel contents. (The elastic scattering feature around 213 nm is heavily overexposed with this scaling.)

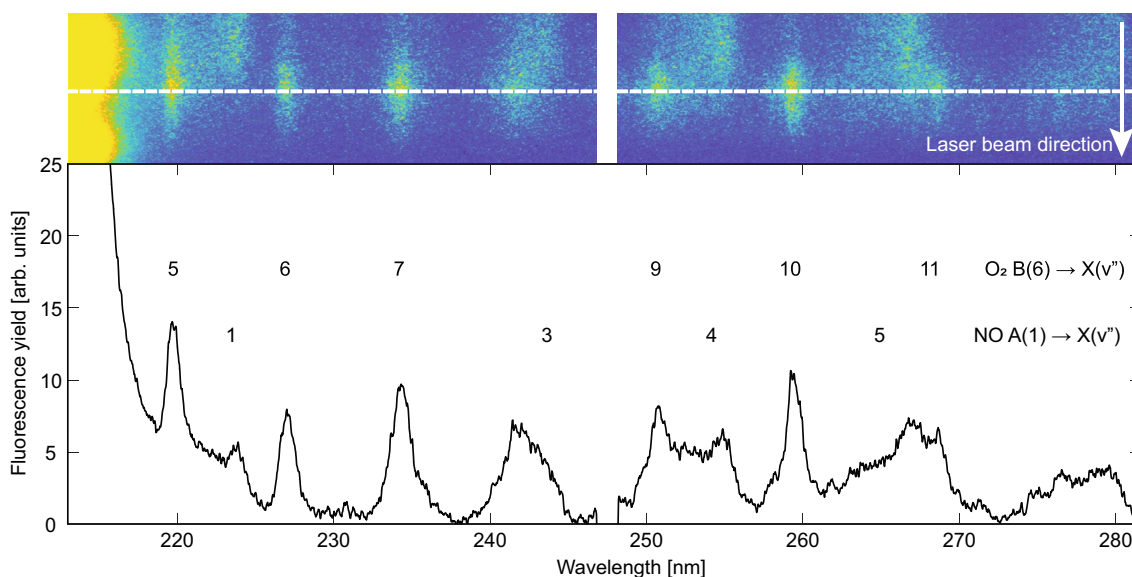


Fig. 7 Fluorescence spectrum of an n-dodecane fuel spray flame recorded under 'Spray A' conditions in a pre-burn combustion vessel, recorded at 65 mm downstream of the nozzle exit. The laser beam passes the field of view top-down. The spectrum is recorded in two runs, of about 30 nm wavelength coverage each, with a small gap in between. Top panels show the average of raw data from 4 (left) or 5 (right) individual fuel spray injections. The bottom of these plots cor-

respond to the spray axis, the white lines indicate the spray boundary at this axial location (65 mm downstream of the nozzle exit), and the height of the plots correspond to 20.9 mm in the object plane. The spectrum in the bottom panel is obtained from column-wise integration of these plots over their full height. Assignment of the most prominent peaks is indicated

the laser beam, due to significant absorption losses (compare also Fig. 6). Further to the red ($\lambda \gtrsim 220$ nm) spectral structure becomes evident. The upper panels of Fig. 7 show that this spectral structure largely originates from two slightly displaced locations at or just outside the spray boundary. At the spray boundary, there are emission features at about 220, 226, 234, 242, 251 and 260 nm; these match well with the expected central emission wavelengths of the stronger members of the $B(v' = 1, 6) \rightarrow X(v'')$ bands in the Schumann-Runge system. The spray periphery is a region where hot oxygen is present, which most likely is excited by our

213-nm radiation in the $1 \leftarrow 2$ and $6 \leftarrow 4$ ($v' \leftarrow v''$) bands of the Schumann-Runge system [29]. The former initial state will be relatively well-populated, but the transition has a small Franck-Condon factor. The $v' = 4$ -state will be less populated, also at high temperature, but the transition has a relatively large Franck-Condon factor, which compensates for the lower population. The relative intensities of the various fluorescence peaks indicate that the fluorescence is in fact originating from the $B(v' = 6)$ state. A little bit further away from the spray axis, weak emission can be seen at about 224, 244, and 256 nm, which can be attributed to the

$A(1) \rightarrow X(v'')$ bands of NO, as before. No fluorescence is observed from the central region of the spray.

4 Conclusion

We have demonstrated laser-induced fluorescence using the 5th harmonic ($\lambda = 213$ nm) of an unseeded, ns-pulsed Nd:YAG laser as a relatively low-cost and uncomplicated tool for the qualitative visualisation of nitric oxide (NO) distributions in a variety of environments. At room temperature, NO gives rise to spectrally well-defined structure, and there is no significant absorption of the excitation laser beam. At higher fluences multi-photon processes give rise to blue-shifted fluorescence. These processes compete with the direct population of the NO A-state, and for diagnostic purposes should be avoided. Contrary to most other NO detection schemes, the signal improves with increasing pressure, which we attribute to improved overlap between laser line shape and absorption line shape with increasing pressure broadening. In hot combustion end gas laser beam attenuation becomes significant, and in the presence of high-temperature oxygen (≈ 1000 K) spectral interference by the Schumann-Runge bands needs to be taken into consideration.

Author contributions T.B. and N.M. performed the measurements. All authors were involved in the data analysis and in writing and reviewing the manuscript.

Data availability statement No datasets were generated or analysed during the current study.

Declarations

Conflict of interest The authors declare no Conflict of interest.

Open Access This article is licensed under a Creative Commons Attribution 4.0 International License, which permits use, sharing, adaptation, distribution and reproduction in any medium or format, as long as you give appropriate credit to the original author(s) and the source, provide a link to the Creative Commons licence, and indicate if changes were made. The images or other third party material in this article are included in the article's Creative Commons licence, unless indicated otherwise in a credit line to the material. If material is not included in the article's Creative Commons licence and your intended use is not permitted by statutory regulation or exceeds the permitted use, you will need to obtain permission directly from the copyright holder. To view a copy of this licence, visit <http://creativecommons.org/licenses/by/4.0/>.

References

1. K. Kohse-Höinghaus, Laser techniques for the quantitative detection of reactive intermediates in combustion systems. *Prog. Energy Combust. Sci.* **20**, 203–279 (1994)
2. W.G. Bessler, C. Schulz, T. Lee, J.B. Jeffries, R.K. Hanson, Strategies for laser-induced fluorescence detection of nitric oxide in high-pressure flames. I. A-X(0,0) excitation. *Appl. Opt.* **41**, 3547–3557 (2002)
3. M. Aldén, J. Bood, Z. Li, M. Richter, Visualization and understanding of combustion processes using spatially and temporally resolved laser diagnostic techniques. *Proc. Combust. Inst.* **33**, 69–97 (2011)
4. P. Eyzat, J.C. Guibet, A new look at nitrogen oxides formation in internal combustion engines. *SAE Transactions 77 Section 1*, 481–500 (1968)
5. G.G.M. Stoffels, E. van den Boom, C. Spaanjaars, N. Dam, W.L. Meerts, J.J. ter Meulen, J.L.C. Duff, D.J. Rickeard, In-cylinder measurements of NO formation in a Diesel engine. *SAE Paper 1999-01-1487* (1999)
6. K. Verbiezen, Quantitative NO measurements in a diesel engine. PhD thesis, Radboud University, Nijmegen, NL (2006)
7. W.G. Bessler, C. Schulz, T. Lee, J.B. Jeffries, R.K. Hanson, Strategies for laser-induced fluorescence detection of nitric oxide in high-pressure flames. II. A-X(0,1) excitation. *Appl. Opt.* **42**, 2031–2042 (2003)
8. W.G. Bessler, C. Schulz, T. Lee, J.B. Jeffries, R.K. Hanson, Strategies for laser-induced fluorescence detection of nitric oxide in high-pressure flames. III. comparison of A-X excitation schemes. *Appl. Opt.* **42**, 4922–4936 (2003)
9. C. Schulz, V. Sick, J. Heinze, W. Stricker, Laser-induced-fluorescence detection of nitric oxide in high-pressure flames with A-X(0,2) excitation. *Appl. Opt.* **36**, 3227–3232 (1997)
10. J. Wormhoudt, J.H. Shorter, C.C. Cook, J.J. Zayhowski, Diode-pumped 214.8-nm Nd:YAG/Cr³⁺:YAG microchip laser system for the detection of NO. *Appl. Opt.* **39**, 4418–4424 (2000)
11. B. Arnold, L. Kelly, J.B. Oleske, A. Schill, Standoff detection of nitrotoluenes using 213-nm amplified spontaneous emission from nitric oxide. *Anal. Bioanal. Chem.* **395**, 349–355 (2009)
12. M.A. Gondal, A.A.I. Khalil, N. Al-Suliman, High sensitive detection of nitric oxide using laser induced photoacoustic spectroscopy at 213 nm. *Appl. Opt.* **51**, 5724–5734 (2012)
13. C. Brackmann, J. Bood, J.D. Naucélér, A.A. Konnov, M. Aldén, Quantitative picosecond laser-induced fluorescence measurements of nitric oxide in flames. *Proc. Combust. Inst.* **36**, 4541–4548 (2017)
14. H. Wu, X. Yin, L. Dong, Z. Jia, J. Zhang, F. Liu, W. Ma, L. Zhang, W. Yin, L. Xiao, S. Jia, F.K. Tittel, Ppb-level nitric oxide photoacoustic sensor based on a mid-ir quantum cascade laser operating at 52°C. *Sens. Actuators, B Chem.* **290**, 426–433 (2019)
15. A.W. Rollins, P.S. Rickly, R.S. Gao, T.B. Ryerson, S.S. Brown, J. Peischl, I. Bourgeois, Single-photon laser-induced fluorescence detection of nitric oxide at sub-parts-per-trillion mixing ratios. *Atmos. Meas. Tech.* **13**, 2425–2439 (2020). <https://doi.org/10.5194/amt-13-2425-2020>
16. K.P. Chatelain, S.B. Rojas Chavez, J. Vargas, D.A. Lacoste, Towards laser-induced fluorescence of nitric oxide in detonation. *Shock Waves* **33**, 179–189 (2023)
17. F.K. Tittel, J.J. Allred, Y. Cao, N.P. Sanchez, W. Ren, W. Jiang, D. Jiang, R.J. Griffin, Quantum cascade laser-based sensor system for nitric oxide detection. *Proc. SPIE* **9370**, 93700–17 (2015)
18. S. Liu, W. Zhu, A comprehensive review on the significant role of N₂O in the transformation of nitrogen oxides during combustion. *J. Energy Inst.* (2024). <https://doi.org/10.1016/j.joei.2024.101678>
19. J. Tian, L. Wang, Y. Xiong, Y. Wang, W. Yin, G. Tian, Z. Wang, Y. Cheng, S. Ji, Enhancing combustion efficiency and reducing nitrogen oxide emissions from ammonia combustion: a comprehensive review. *Process Saf. Environ. Prot.* **183**, 514–543 (2024)
20. C.D. Davis, *Lasers and Electro-Optics* (Cambridge University Press, Cambridge (UK), 1996)

21. J. Luque, D.R. Crosley, LIFBASE, database and spectral simulation for diatomic molecules (v. 2.1.1.). Technical Report MP-99-009, SRI International (1999)
22. R.A.L. Tolboom, N.J. Dam, J.J. ter Meulen, J.M. Mooij, J.D.M. Maassen, Quantitative imaging through a spectrograph. 1 principles and theory. *Appl. Opt.* **43**, 5669–5680 (2004)
23. M.D. Di Rosa, R.K. Hanson, Collision broadening and shift of NO $\gamma(0, 0)$ absorption lines by O₂ and H₂O at high temperatures. *J. Quant. Spectrosc. Radiat. Transfer* **52**, 515–529 (1994)
24. R.W.B. Pearse, A.G. Gaydon, *The Identification of Molecular Spectra* (Chapman and Hall, London, 1976)
25. M. Meijer, J. Galle, L.M.T. Somers, J.G.H. van Griensven, S. Verhelst, High-speed characterization of ECN Spray A using various diagnostic techniques. *SAE Int. J. Engines* **6**, 1238–1248 (2012)
26. N. Maes, M. Meijer, N. Dam, B. Somers, H. Baya Toda, G. Bruneaux, S.A. Skeen, L.M. Pickett, J. Manin, Characterization of spray a flame structure for parametric variations in ecn constant-volume vessels using chemiluminescence and laser-induced fluorescence. *Comb. Flame* **174**, 138–151 (2016)
27. C. Schulz, J.B. Jeffries, D.F. Davidson, J.D. Koch, J. Wolfrum, R.K. Hanson, Impact of UV absorption by CO₂ and H₂O on NO-LIF in high-pressure combustion applications. *Proc. Combust. Inst.* **29**, 2735–2742 (2002)
28. Engine Combustion Network internet library. National technology and engineering solutions of SANDIA (2018) <http://www.sandia.gov/ecn/>
29. P.H. Kruppenie, The spectrum of molecular oxygen. *J. Phys. Chem. Ref. Data* **1**, 423–534 (1972)

Publisher's Note Springer Nature remains neutral with regard to jurisdictional claims in published maps and institutional affiliations.